2015 IEEE International Conference on Robotics and Automation (ICRA)
Washington State Convention Center
Seattle, Washington, May 26-30, 2015

Fusing ultra-wideband range measurements with accelerometers and rate gyroscopes for quadrocopter state estimation

Mark W. Mueller, Michael Hamer, and Raffaello D'Andrea

Abstract— **A state estimator for a quadrocopter is presented, using measurements from an accelerometer, angular rate gyroscope, and a set of ultra-wideband ranging radios. The estimator uses an extended aerodynamic model for the quadrocopter, where the full 3D airspeed is observable through accelerometer measurements. The remaining quadrocopter states, including the yaw orientation, are rendered observable by fusing ultra-wideband range measurements, under the assumption of no wind. The estimator is implemented on a standard microcontroller using readily-available, low-cost sensors. Performance is experimentally investigated in a variety of scenarios, where the quadrocopter is flown under feedback control using the estimator output.**

I. Introduction

Quadrocopters offer agile and mechanically simple testbeds for research on flying robots. They also promise to be useful for commercial applications, for example as package delivery robots [1] or as mobile sensing platforms.

State estimation is a fundamental requirement for the autonomous operation of these vehicles. Typical estimation strategies fuse a variety of sensors, typically combining inertial measurement units with sensors providing absolute measurements.

A number of solutions for absolute state measurement currently exist. Off-board vision is often used to measure the position and orientations of flying vehicles, using either commercial motion-capture systems [2]–[4], or lower-cost cameras [5], [6]. On-board vision systems are also very popular, with [7]–[9] being examples of monocular-, and [10], [11] of stereo-vision systems. Finally, many outdoor systems rely on GPS systems for position measurements, as e.g. [12]. These different localisation solutions present different trade-offs between cost, measurement accuracy, robustness to external influences, computational burden, and ease of deployment.

A relatively new method of indoor localization utilizes low cost, low power, ultra-wideband (UWB) radio modules to estimate inter-module distance by measuring the transmission and reception time of UWB pulses, see e.g. [13]–[15]. This paper presents a quadrocopter state estimation strategy, which uses these range measurements to localize the quadrocopter. This is enabled by a mobile UWB radio connected to the quadrocopter and a set of fixed modules with known position (anchors) placed in the environment. Inter-module distance is measured using a time-of-arrival (TOA) approach. The layout of the system is illustrated in Fig. 1.

This paper demonstrates that closed loop control of a quadrocopter during agile manoeuvres is possible using UWB range measurements fused with a dynamic model of the quadrocopter and with measurements from on-board accelerometers and rate gyroscopes. The state estimator, controller, and trajectory generator all run on-board the quadrocopter's microcontroller.

The remainder of this paper is organised as follows: the dynamics of the quadrocopter are presented in Section II, with a special focus on aerodynamic effects. Section III then presents sensor models for each of the three sensors used, and Section IV presents a state estimator fusing these measurements with a dynamic model of the quadrocopter. An algorithm to estimate the range between two UWB radios is then given in Section V. The approach is validated in experiment in Section VI, and the paper concludes with Section VII.

II. System dynamics

This section presents the equations of motion governing the flight of a quadrocopter. These equations will later be used in the prediction step of the state estimator. Furthermore, specific attention will be paid to an accelerometer model, showing how the vehicle's three dimensional velocity may be directly inferred from the accelerometer measurement.

The quadrocopter is modelled as a rigid body, governed by the Newton-Euler equations [16]. Denoting the quadrocopter's position in an inertial reference frame with $\boldsymbol{x}$ and the orientation of the quadrocopter's body with respect to the inertial reference frame with $\mathbf{R}$, the equations of motion

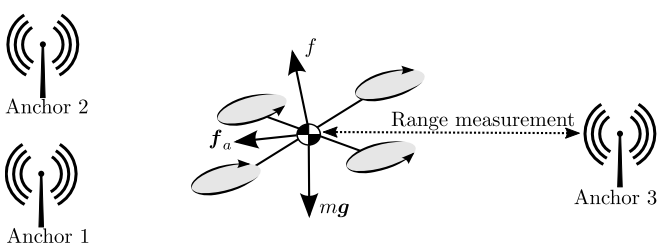

Fig. 1. A quadrocopter uses time of flight measurements from an UWB radio to measure the distance to a set of stationary UWB anchors in a round-robin fashion. An accelerometer effectively measures the static thrust f and other aerodynamic effects $\boldsymbol{f}_a$, thereby providing information on the quadrocopter's translational velocity. Rate gyroscopes are used to measure the quadrocopter's angular velocity.

The authors are with the Institute for Dynamic Systems and Control, ETH Zurich, Sonneggstrasse 3, 8092 Zurich, Switzerland.
{mwm, hamerm, rdandrea}@ethz.ch

of the quadrocopter are as below. The total thrust produced by the propellers is written as f, and the acceleration due to gravity is expressed as $\boldsymbol{g}$. All remaining aerodynamic effects are captured in the vector $\boldsymbol{f}_a$, whose components are expressed in the body-fixed frame. The vehicle's mass is given by m, and $\boldsymbol{e}_3 = (0, 0, 1)$. The notation (x, y, z) will be used throughout this paper to compactly express the elements of a vector. The forces are illustrated in Fig. 1.

$$m\ddot{\boldsymbol{x}} = \mathbf{R}\ (f\boldsymbol{e}_3 + \boldsymbol{f}_a) + m\boldsymbol{g} \tag{1}$$

$$\dot{\mathbf{R}} = \mathbf{R}\,[\![\boldsymbol{\omega}\times]\!] \tag{2}$$

Note that this uses the matrix form of the cross product, given by

$$[\![\boldsymbol{\omega}\times]\!] = \begin{bmatrix} 0 & -\omega_3 & \omega_2 \\ \omega_3 & 0 & -\omega_1 \\ -\omega_2 & \omega_1 & 0 \end{bmatrix} \tag{3}$$

where $\boldsymbol{\omega} = (\omega_1, \omega_2, \omega_3)$ is the angular velocity of the quadrocopter as expressed in the body fixed frame.

The angular acceleration of the quadrocopter evolves as a function of the torques acting on the vehicle, the current angular velocity, and the quadrocopter's inertia. These equations are given for example in [17], and will not be repeated here as these equations are not required for the estimator design in Section IV.

A. Static thrust force

It is assumed that the angular velocity $\dot{\theta}_i$ of each propeller i is known, for example as a measurement returned by the electronic speed controller. The thrust produced by a stationary propeller may be modelled as quadratic in its angular velocity, with proportionality constant κ [18], so that the total thrust of the the vehicle is

$$f = \sum_{i=1}^{4} \kappa \dot{\theta}_i^2. \tag{4}$$

This static thrust points along the propellers' axis of rotation.

B. Aerodynamic effects

The force generated by a propeller translating with respect to the free stream will typically be significantly different from the static thrust force f. This deviation is given by $\boldsymbol{f}_a$, which is taken to be a function of the quadrocopter's relative airspeed.

The effect of the component of the airspeed in the rotor plane is well documented, e.g. [17], [19]–[21]. Typically, blade flapping is invoked to motivate a linear dependence between the quadrocopter's velocity in the rotor plane to the components of $\boldsymbol{f}_a$ in the rotor plane.

There is rich literature on the aerodynamics of propellers translating along their axial directions [22], typically in the context of large, fixed-wing aeroplanes. The dependence of the thrust produced by a quadrocopter translating in the thrust direction has also been studied in the literature, for example [23], [24].

Here, the aerodynamic force is modelled as an interaction between the rotating propellers, and the vehicle's airspeed. The force is assumed to be linear in the product of the airspeed and the propeller speeds, with $\kappa_\perp$ the proportionality constant for the force in the plane of the rotors, and $\kappa_\parallel$ the proportionality constant in the direction of the thrust vector. It is assumed that there is no wind, so that the quadrocopter's relative airspeed equals the quadrocopter's velocity with respect to the inertial frame.

The force can then be calculated as

$$\boldsymbol{f}_a = \mathbf{K}_{\text{aero}}\, \dot{\theta}_\Sigma\, \mathbf{R}^{-1} \dot{\boldsymbol{x}} \tag{5}$$

where

$$\mathbf{K}_{\text{aero}} = \text{diag}\left(\kappa_\perp, \kappa_\perp, \kappa_\parallel\right) \tag{6}$$

$$\dot{\theta}_\Sigma = \sum_{i=1}^{4} \left|\dot{\theta}_i\right|. \tag{7}$$

III. Sensors

The estimator presented in Section IV relies on the measurements of three distinct types of sensors: angular rate gyroscopes, accelerometers, and UWB range sensors. Each of these sensors will be briefly discussed here, and the sensor output will be linked to the quadrocopter dynamics of Section II.

A. Angular rate gyroscopes

The angular rate gyroscopes measure the quadrocopter's angular velocity in the body frame. The measurement will be modelled here as

$$\boldsymbol{z}_{\text{gyro}} = \boldsymbol{\omega} + \boldsymbol{\eta}_{\text{gyro}} \tag{8}$$

where $\boldsymbol{\eta}_{\text{gyro}}$ is assumed to be zero-mean white noise. More complete models exist, which include for example scale errors or biases [25], here however it will be assumed that the sensor is well calibrated and these effects may be neglected.

B. Accelerometers

An accelerometer measures the specific acceleration of a body, that is the difference between the acceleration and gravitational acceleration, as expressed in the body frame. A good tutorial may be found in [21].

The accelerometer measurements are assumed to be corrupted by zero-mean white noise $\boldsymbol{\eta}_{\text{acc}}$ so that the accelerometer measurement can be derived from (1) as

$$\boldsymbol{z}_{\text{acc}} = \mathbf{R}^{-1}\left(\ddot{\boldsymbol{x}} - \boldsymbol{g}\right) + \boldsymbol{\eta}_{\text{acc}} = \frac{1}{m}\left(\boldsymbol{e}_3 f + \boldsymbol{f}_a\right) + \boldsymbol{\eta}_{\text{acc}}. \tag{9}$$

Thus, given knowledge of the propellers' angular velocities and through (4) the static thrust force f, the accelerometer yields information about the aerodynamic force $\boldsymbol{f}_a$. This will be exploited in the design of the estimator, as it renders all three components of the vehicle's airspeed observable.

C. UWB range measurements

The UWB radio mounted on the quadrocopter uses a TOA-based algorithm, presented in Section V, to calculate the distance between the quadrocopter at position $\boldsymbol{x}$ and an anchor i at position $\boldsymbol{p}_{\text{uwb,i}}$. This measurement is assumed to be a perfect measurement of distance, corrupted by zero mean white noise η_{uwb}, such that the measurement is given as

$$z_{\text{uwb,i}} = \left\| \boldsymbol{p}_{\text{uwb,i}} - \boldsymbol{x} \right\| + \eta_{\text{uwb}} \tag{10}$$

where $\|\cdot\|$ represents the Euclidean norm.

IV. State estimator

An extended Kalman filter is used to estimate the state of the quadrocopter in flight. This section will present the necessary equations for the Kalman filter, derived from the system's dynamic model of Section II and the sensor models of Section III.

To estimate the state of the quadrocopter the estimator will use sensor measurements from the accelerometer, angular rate gyroscope, and the UWB range sensors, and combine these with the motor commands. Throughout this section, a caret will be used to indicate an estimate, for example $\hat{\boldsymbol{\omega}}$ is the estimate of the body's angular velocity.

The goal of the estimator is to estimate the twelve-dimensional state of the rigid body, consisting of the quadrocopter's position, velocity, orientation, and angular velocity. The estimation is split into two parts: estimating the vehicle's angular velocity, and estimating the remaining states. As the computational complexity of a Kalman filter scales approximately as n^3, where n is the number of states [26], this reduces the computational cost to estimate the twelve states by more than 50%.

For the sake of brevity, the standard Kalman filter equations available in a standard reference (such as [26]) will not be repeated in this paper. Instead the focus will be on the system dynamics equations, and on the measurement equations.

The angular rate gyroscope measurement is used directly as the estimate of the quadrocopter's angular velocity, so that

$$\hat{\boldsymbol{\omega}} = \boldsymbol{z}_{\text{gyro}}. \tag{11}$$

This bases on the assumption that the measurement noise of the rate gyroscopes is negligible. The covariance of this estimate is equal to the covariance of $\boldsymbol{\eta}_{\text{gyro}}$.

An extended Kalman filter is used to estimate the quadrocopter's position, velocity, and orientation. The estimator has a nine-dimensional stochastic state ξ:

$$\xi = \left(\boldsymbol{x}, \boldsymbol{\rho}, \boldsymbol{\delta} \right). \tag{12}$$

where $\boldsymbol{x}$ is the quadrocopter's position expressed in the inertial coordinate system, and $\boldsymbol{\rho} = \mathbf{R}^{-1}\dot{\boldsymbol{x}}$ is the velocity of the quadrocopter expressed in the body frame. The three dimensional vector $\boldsymbol{\delta}$ is an attitude error representation, used to encode the uncertainty about the vehicle's orientation.

In addition to the stochastic state, the estimator also contains a reference orientation $\mathbf{R}_{\text{ref}}$. The reason for this parametrisation is as follows: although the orientation of one frame with respect to another contains only three degrees of freedom, there exists no global three-dimensional representation without singular points [27]. Thus, when using a three dimensional representation alone (such as Euler angles), the estimator will have to deal with singularities. However, using parametrisations with more than three elements (such as the four dimensional Euler symmetric parameters, or the nine dimensional rotation matrix) requires applying constraints, which would in turn imply rank deficiency in the associated covariance matrix [28]. Higher dimensional representations also imply a higher computational cost.

For this reason, the estimated attitude is encoded using both the reference orientation and the three attitude error components. The error components are assumed to be infinitesimal, and then the estimator's attitude estimate is given as below [16], where all orientations are expressed with rotation matrices:

$$\hat{\mathbf{R}} = \hat{\mathbf{R}}_{\text{ref}} \left(\mathbf{I} + [\![\hat{\boldsymbol{\delta}} \times]\!] \right) \tag{13}$$

with $\mathbf{I} \in \mathbb{R}^{3\times 3}$ the identity matrix. This formulation is sometimes referred to as a multiplicative Kalman filter, and the key idea is to maintain the orientation estimate in the reference attitude, use the three attitude error components to encode the covariance associated with the orientation. After each Kalman filter step, the reference rotation is updated with the attitude errors, and $\hat{\boldsymbol{\delta}}$ is reset to zero. The covariance is left unchanged during this reset step. More information on this approach can be found in e.g. [29].

A. Prediction equations

During the Kalman filter prediction step, the estimated states evolve as follows, from Section II:

$$\dot{\hat{\boldsymbol{x}}} = \hat{\mathbf{R}}_{\text{ref}} \left(\mathbf{I} + [\![\hat{\boldsymbol{\delta}} \times]\!] \right) \hat{\boldsymbol{\rho}} \tag{14}$$

$$\dot{\hat{\boldsymbol{\rho}}} = \frac{1}{m} f \boldsymbol{e}_3 + \left(\frac{1}{m} \mathbf{K}_{\text{aero}} \dot{\theta}_{\Sigma} - [\![\hat{\boldsymbol{\omega}} \times]\!] \right) \hat{\boldsymbol{\rho}} - \|\boldsymbol{g}\| \left(\mathbf{I} - [\![\hat{\boldsymbol{\delta}} \times]\!] \right) \hat{\mathbf{R}}_{\text{ref}}^{-1} \boldsymbol{e}_3 \tag{15}$$

$$\dot{\hat{\boldsymbol{\delta}}} = \hat{\boldsymbol{\omega}} \tag{16}$$

$$\dot{\hat{\mathbf{R}}}_{\text{ref}} = 0 \tag{17}$$

The angular rate gyroscope is used as an input to this system, entering through (16). The zero-mean noise on the rate gyroscope is then trivially encoded as process noise using the standard extended Kalman filter formulation [26]. Additionally, a zero-mean acceleration is assumed to act on the system, so that an additional three dimensional process noise is taken to act upon $\boldsymbol{\rho}$.

By stacking (14)-(16), taking the derivative with respect to ξ, and evaluating at the filter's current estimate $\hat{\xi}$ and $\hat{\mathbf{R}}_{\text{ref}}$, the Jacobian necessary for performing the Kalman filter covariance prediction can be computed.

B. Accelerometer measurement update equation

The accelerometer allows to infer the vehicle's airspeed, through the aerodynamic forces. It is assumed that the propellers' angular rates $\dot{\theta}_i$ are known, so that the static thrust f can be computed. This can then be subtracted from the accelerometer measurement, so that the result $\tilde{\boldsymbol{z}}_{\text{acc}}$ is a measurement of $\boldsymbol{f}_a$, scaled by the vehicle mass and corrupted by noise, by (9) and (5):

$$\begin{aligned}\tilde{\boldsymbol{z}}_{\text{acc}} &= \boldsymbol{z}_{\text{acc}} - \frac{1}{m}\boldsymbol{e}_3\kappa\sum_{i=1}^{4}\dot{\theta}_i = \frac{1}{m}\boldsymbol{f}_a + \boldsymbol{\eta}_{\text{acc}} \\ &= \frac{1}{m}\mathbf{K}_{\text{aero}}\,\dot{\theta}_\Sigma\,\boldsymbol{\rho} + \boldsymbol{\eta}_{\text{acc}}\end{aligned} \tag{18}$$

which is linear in the quadrocopter's airspeed, and may thus be easily encoded in the Kalman filter.

C. UWB range measurement update equation

A range measurement to an anchor can be modelled by (10). This may again easily be linearised about the estimator's current state, and incorporated in the filter.

1) Ranging outlier rejection: Outliers from the UWB ranging radios may be detected by computing likelihood of a given ranging measurement. Because the measurements are scalar, the resulting innovation covariance [26] will also be scalar, and may thus be inverted at low computational cost. Squaring the difference between the actual range measurement and the measurement expected given the current state estimate, and multiplying by the inverse innovation yields a squared normalised distance called the Mahalanobis distance [26]. The larger this normalised distance the less likely a particular measurement is to result from the statistical properties of the expected error. A measurement with a distance larger than some given threshold may thus be rejected as an outlier.

V. Range measurement using time-of-arrival measurements

As discussed in Section III-C, a UWB radio mounted to the quadrocopter is used to measure distances to anchors placed within the environment. Many different methods exist to measure distance using UWB radio [13], [30]–[32]; for the purposes of this paper, a TOA-based method known as two way ranging is used [31].

A. The two way ranging algorithm

The high temporal resolution of UWB pulses enables accurate range measurement; however, it also poses challenges, such as compensating for clock frequency differences between UWB modules [13], [30]. Compensating for these differences is achieved using a variation of the two way ranging algorithm, which employs a repeated reply to allow measurement of anchor delay relative to the quadrocopter's clock [31].

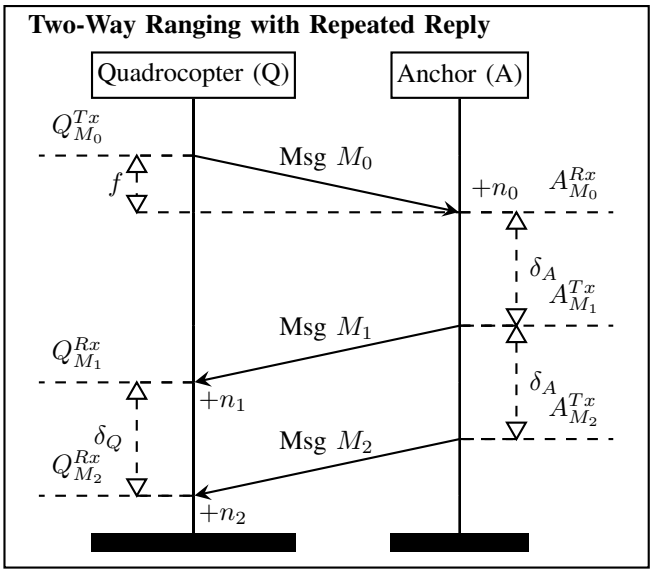

Fig. 2. A two-way ranging with repeated reply algorithm is used to measure the time of flight between a quadrocopter and an anchor. By subtracting the locally-measured processing time ($Q^{Rx}_{M_2} - Q^{Rx}_{M_1}$) from the round-trip time ($Q^{Rx}_{M_1} - Q^{Tx}_{M_0}$), the time of flight ($f$) can be estimated in the quadrocopter's local clock.

1) Measurement of clock frequency difference: As shown in Fig. 2, after sending its first reply, the anchor waits for a predetermined amount of time $\delta_A = \delta$, where δ is a predefined constant, here chosen as 1 ms. After this time delay, the anchor's reply message is repeated, allowing the anchor's delay to be measured by the quadrocopter as

$$z_{\delta_Q} = \delta_Q + n_2 - n_1 = Q^{Rx}_{M_2} - Q^{Rx}_{M_1}, \tag{19}$$

where n_i are samples of a noise distribution and affect the reception timestamp. Fig. 3 shows the difference between the anchor's delay and the expected delay, as measured by the quadrocopter ($\delta_Q - \delta$). This measurement is time-varying due to clock frequency drift and is affected by noise.

It is assumed that the noise term $n_2 - n_1$ is zero mean, and thus δ_Q tracks the mean of the time-varying measurements. By applying a low-pass filter over successive measurements, δ_Q can thus be estimated as $\hat{\delta}_Q$. Analysing the distribution of the noise term $n_2 - n_1$ around this estimate showed that this term is uncorrelated between distance measurements and distributed with standard deviation 0.17 ns. Fig. 3 further shows the existence of outliers, which motivates the inclusion of outlier detection as previously discussed in Section IV-C.

2) Time of flight measurement: Using the estimate $\hat{\delta}_Q$, the quadrocopter is able to measure the time of flight f as

$$z_{\text{TOF}} = f + \frac{n_1 + n_0}{2} = \frac{Q^{Rx}_{M_1} - Q^{Tx}_{M_0} - \hat{\delta}_Q}{2}. \tag{20}$$

Multiplying the time of flight by the speed of light c and comparing with (10) yields

$$\begin{aligned}z_{\text{uwb}} &= cf + \frac{c}{2}(n_1 + n_0) \\ &= \left\|\boldsymbol{p}_{\text{uwb,i}} - \boldsymbol{x}\right\| + \eta_{\text{uwb}}\end{aligned} \tag{21}$$

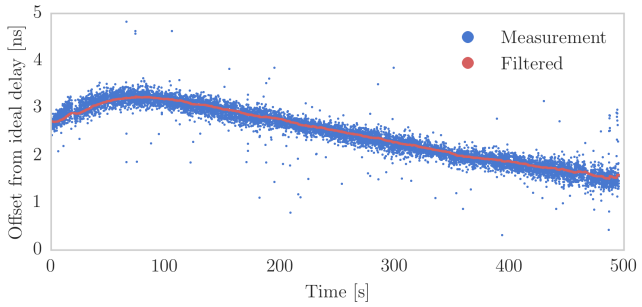

Fig. 3. A plot showing the difference between the anchor's delay and the expected delay, as measured by the quadrocopter. In the ideal case, this would equal zero; the discrepancy is due to a difference in clock frequencies between the quadrocopter and anchor. This function is time varying, due to clock frequency drift, and is corrupted by an uncorrelated noise with standard deviation 0.17 ns. Note that 1 ns corresponds to a distance measurement error of 30 cm.

Assuming the noise term $n_1 + n_0$ has the same statistical properties as $n_2 - n_1$, we conclude that η_{uwb} is zero mean with standard deviation 0.025 m. This result was experimentally verified by recording range measurements at a constant distance and calculating their statistical properties. Furthermore, this result reflects a similar analysis performed in [32].

VI. Experimental validation

The estimation approach is validated in experiment in the Flying Machine Arena [4]. Ascending Technologies Hummingbird quadrocopters [33] are used, modified to use the Pixhawk PX4 flight management unit [10]. The estimator is implemented in C++ and runs on the microcontroller on the flight management unit.

The flight management unit features a three axis accelerometer and gyroscope, each sampled at 1000Hz for the estimator.

Six UWB radios were used for the experiments: one mounted on the quadrocopter, and five used as anchors. Of the anchors, three were placed in an approximately isosceles triangle on the floor, and two were placed at a height of approximately 1.7 m above the ground. At 200 Hz the quadrocopter requests a range to an anchor, starting at the first anchor and proceeding sequentially.

A controller also runs on the microcontroller, which computes desired motor angular velocities as a function of the estimator's state, and a desired state. A position setpoint is periodically transmitted to the vehicle from a base station over a dedicated wireless channel.

The Flying Machine Arena is additionally equipped with an overhead motion capture system, which measures the position and orientation of the quadrocopter at 200Hz, with precision on the order of millimetres and degrees, respectively. The output from this motion capture system is used as ground truth for these experiments. Note that the quadrocopter's closed loop control is based solely on the output of the presented estimator, and the motion capture system is used exclusively for performance evaluation.

A. Estimator parameters

The quadrocopter has a mass of 0.56 kg. The propeller force coefficient is given by $\kappa = 6.41\,\mu\text{N}\,\text{s}^2\,\text{rad}^{-2}$.

The aerodynamic force coefficients $\kappa_{\parallel}$ and $\kappa_{\perp}$ were estimated by analysing data from quadrocopter flights in the Flying Machine Arena. The coefficients are estimated as:

$$\kappa_{\perp} = 0.000\,11\,\text{N}\,\text{s}^2\,\text{rad}^{-1}\,\text{m} \tag{22}$$

$$\kappa_{\parallel} = 0.000\,23\,\text{N}\,\text{s}^2\,\text{rad}^{-1}\,\text{m}. \tag{23}$$

The noise covariance for the angular rate gyroscope and the accelerometer were set as follows:

$$\text{Var}\left(\boldsymbol{\eta}_{\text{gyro}}\right) = \text{diag}\left(0.01, 0.01, 0.25\right)\text{rad}^2\,\text{s}^{-2} \tag{24}$$

$$\text{Var}\left(\boldsymbol{\eta}_{\text{acc}}\right) = \text{diag}\left(9, 9, 81\right)\text{m}^2\text{s}^{-4} \tag{25}$$

These covariances are partly based on experimental data, which showed a significantly higher accelerometer noise in the direction of the quadrocopter's thrust, and partly on experimental tuning. The observed higher noise in the direction of the thrust could possibly be explained by the quadocopter's asymmetric mechanical structure, and the transmission of vibrations.

The covariance of the UWB range measurements was set to $\text{Var}\left(\eta_{\text{uwb}}\right) = 0.0625\,\text{m}^2$. This is an order of magnitude larger than suggested in Section V, however due to a possible unmodelled measurement bias (discussed further in this section), was necessary for smooth flight. The Mahalanobis distance for rejecting a UWB range measurement was set to 3.

The acceleration process noise acting to increase the estimator's covariance in the prediction state of the Kalman filter was set to $9\,\mathbf{I}\,\text{m}^2/\text{s}^{-4}$.

B. Experiments

Three different experiments were performed: hovering in one spot for an extended period of time, flying a slow vertical manoeuvre, and flying a fast horizontal manoeuvre. The experiments are shown in Fig. 4, and each experiment is shown in the attached video. Errors are quantified by their mean (ϵ_μ) and standard deviation (ϵ_σ) – these are related to the root-mean-squared (RMS) error (ϵ_{RMS}) as $\epsilon_{\text{RMS}}^2 = \epsilon_\mu^2 + \epsilon_\sigma^2$ [26].

1) Hovering: The quadrocopter was commanded to hold a position in space for a period of 13 minutes. The quadrocopter's yaw angle (that is, the rotation about the thrust axis) was commanded to be constant throughout this period.

The mean position estimation error was approximately 50 mm in the horizontal direction, and 244 mm in the vertical direction. The standard deviation of the error was 36 mm horizontally and 53 mm vertically.

The RMS closed loop position tracking error was 302 mm, and the RMS closed loop yaw tracking error was 5.3°.

2) Slow vertical manoeuvre: A second experiment was performed where the quadrocopter flies along a vertically oriented rectangle of size 3.5×3 m. The position setpoint was moved along slowly at $1\,\text{m}\,\text{s}^{-1}$ to minimize the influence dynamic effects, and interactions of the controller.

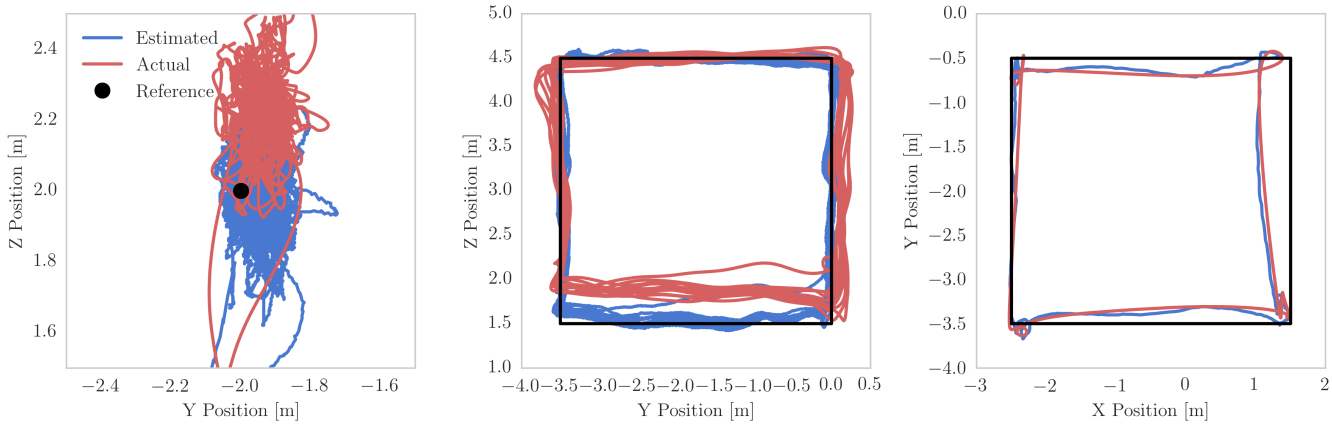

Fig. 4. Three experiments evaluating the quadrocopter performance under feedback control using the estimator, from left to right: the quadrocopter hovers at a position for 13 minutes; the quadrocopter flies a slow vertical manoeuvre; and the quadrocopter flies a fast horizontal manoeuvre. Gravity points along negative Z. For the hover experiment, the results were comparable in both horizontal directions, therefore only the Y-Z plane is shown – a history of the estimation errors is given in Fig. 5. The standard deviation of the estimation error during the hover experiment was 36 mm horizontally, and 53 mm vertically, with the corresponding mean values of 50 mm and 244 mm, respectively. The setpoint was moved at a constant $1\,\mathrm{m\,s^{-1}}$ during the slow manoeuvre, and the result clearly shows systematic biases present in the system, especially along the lower edge of the trajectory. The maximum speed along the fast trajectory was $3.4\,\mathrm{m\,s^{-1}}$. Eleven sequential rounds of the fast trajectory were flown, however only one is shown. The attached video shows each of the experiments.

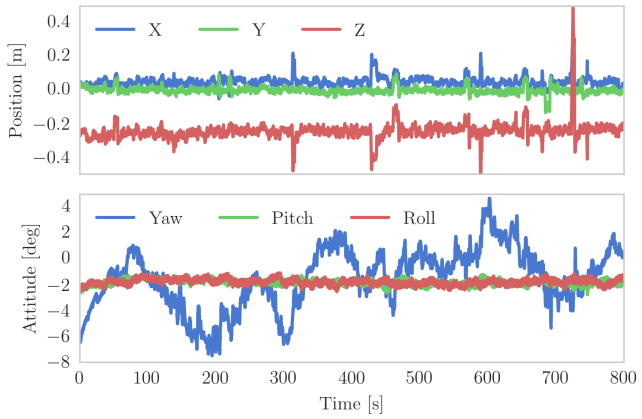

Fig. 5. The estimation error over approximately 13 minutes of hovering. The actual and estimated position trajectories are shown in Fig. 4. The attitude error is reported as differences in the true and estimated Z-Y-X yaw-pitch-roll angles [16].

The quadrocopter flew twelve times along the rectangle. A discussion of the system's performance is given below.

3) Fast horizontal manoeuvre: The performance of the estimator during more dynamic trajectories was investigated by having the quadrocopter fly along a $4 \times 3\,\mathrm{m}$ horizontal rectangle. Trajectories to the corners were generated using the method of [34], with the quadrocopter commanded to start and end at rest, at the corners. The duration along the long edge of the rectangle was 2.2 s, and along the short edge 1.9 s, so that the maximum commanded velocity along the trajectory is $3.4\,\mathrm{m\,s^{-1}}$. Over 11 rounds around the rectangle, the position estimation error had a mean of 41 mm, and standard deviation of 123 mm. One such round around the rectangle is shown in Fig. 4, and the attached video visualises an ensemble of such rounds.

4) Discussion and interpretation: The experimental results show that the quadrocopter's full state is observable to the state estimator. Specifically it appears that the quadrocopter's corrective motions when holding a constant position set point are sufficient for observing the quadrocopter's orientation about its thrust axis, also over prolonged periods of time.

Both the hover experiment, and the slow vertical experiment, showed significant non-zero-mean estimation errors in position. For the vertical rectangle, as can be clearly seen in Fig. 4, there is a significant systematic vertical estimation error along the lower edge of the rectangle. The relatively large mean position estimation errors (on the order of 250 mm) stand in contrast to the much lower standard deviation on the position estimate (64 mm when hovering, and 123 mm along the fast horizontal rectangle).

These systematic estimation errors are most likely explained by systematic errors in the UWB ranging system. Systematic ranging errors could be due to the effects of occlusion and multi-path on the radio signal [35], however the experimental setup had no occlusions. An alternative explanation is given in [14], [36], where the group-delay of an antenna, corresponding to a time-delay of the signal, is a function of antenna orientation. This appears to match the observation that the magnitude and direction of the estimation errors vary as a function of the position in space.

VII. Conclusion

The strategy presented in this paper utilises accelerometers, gyroscopes, and ultra-wideband radios to estimate the dynamic state of a quadrocopter, under the assumption of no wind. The estimator is shown to perform sufficiently well for the quadrocopter to maintain a position for an extended period of time, and to fly dynamic manoeuvres.

Furthermore, the computational complexity is low enough that the estimator may be run on a typical microcontroller.

Inertial measurement sensors are already widely used on flying vehicles, and ultra-wideband radios may be added at low cost and at little additional mass. This system thus appears to be a low-cost, easily-implementable method to improve the autonomy of quadrocopter systems.

ACKNOWLEDGEMENT

The Flying Machine Arena is the result of contributions of many people, a full list of which can be found at `http://www.idsc.ethz.ch/Research_DAndrea/FMA/participants`.

This research was supported by the Swiss National Science Foundation (SNSF) and the NCCR Digital Fabrication (Agreement # 51NF40-141853), also funded by the SNSF.

REFERENCES

[1] R. D'Andrea, "Can drones deliver?" *IEEE Transactions on Automation Science and Engineering*, vol. 11, no. 3, pp. 647–648, 2014.

[2] J. How, B. Bethke, A. Frank, D. Dale, and J. Vian, "Real-time indoor autonomous vehicle test environment," *IEEE Control Systems Magazine*, vol. 28, no. 2, pp. 51–64, April 2008.

[3] N. Michael, D. Mellinger, Q. Lindsey, and V. Kumar, "The GRASP multiple micro-UAV testbed," *IEEE Robotics Automation Magazine*, vol. 17, no. 3, pp. 56 –65, September 2010.

[4] S. Lupashin, M. Hehn, M. W. Mueller, A. P. Schoellig, M. Sherback, and R. D'Andrea, "A platform for aerial robotics research and demonstration: The Flying Machine Arena," *Mechatronics*, vol. 24, no. 1, pp. 41 – 54, 2014.

[5] S. Klose, J. Wang, M. Achtelik, G. Panin, F. Holzapfel, and A. Knoll, "Markerless, vision-assisted flight control of a quadrocopter," in *IEEE/RSJ International Conference on Intelligent Robots and Systems (IROS)*. IEEE, 2010, pp. 5712–5717.

[6] C. Martínez, P. Campoy, I. Mondragón, and M. A. Olivares-Méndez, "Trinocular ground system to control UAVs," in *IEEE/RSJ International Conference on Intelligent Robots and Systems (IROS)*. IEEE, 2009, pp. 3361–3367.

[7] S. Weiss, M. W. Achtelik, S. Lynen, M. C. Achtelik, L. Kneip, M. Chli, and R. Siegwart, "Monocular vision for long-term micro aerial vehicle state estimation: A compendium," *Journal of Field Robotics*, vol. 30, no. 5, pp. 803–831, 2013.

[8] J. Engel, J. Sturm, and D. Cremers, "Camera-based navigation of a low-cost quadrocopter," in *IEEE/RSJ International Conference on Intelligent Robots and Systems (IROS)*. IEEE, 2012, pp. 2815–2821.

[9] I. Sa and P. Corke, "100Hz onboard vision for quadrotor state estimation," in *Australasian Conference on Robotics & Automation*, 2012.

[10] L. Meier, P. Tanskanen, L. Heng, G. Lee, F. Fraundorfer, and M. Pollefeys, "PIXHAWK: A micro aerial vehicle design for autonomous flight using onboard computer vision," *Autonomous Robots*, vol. 33, no. 1-2, pp. 21–39, 2012.

[11] K. Schauwecker and A. Zell, "On-board dual-stereo-vision for autonomous quadrotor navigation," in *International Conference on Unmanned Aircraft Systems (ICUAS)*. IEEE, 2013, pp. 333–342.

[12] G. M. Hoffmann, H. Huang, S. L. Waslander, and C. J. Tomlin, "Precision flight control for a multi-vehicle quadrotor helicopter testbed," *Control engineering practice*, vol. 19, pp. 1023–1036, June 2011.

[13] S. Gezici, Z. Tian, G. Giannakis, H. Kobayashi, A. Molisch, H. Poor, and Z. Sahinoglu, "Localization via ultra-wideband radios: a look at positioning aspects for future sensor networks," *IEEE Signal Processing Magazine*, vol. 22, no. 4, pp. 70–84, 2005.

[14] M. Mahfouz, C. Zhang, B. Merkl, M. Kuhn, and A. Fathy, "Investigation of high-accuracy indoor 3-D positioning using UWB technology," *IEEE Transactions on Microwave Theory and Techniques*, vol. 56, no. 6, pp. 1316–1330, 2008.

[15] A. Prorok, A. Arfire, A. Bahr, J. R. Farserotu, and A. Martinoli, "Indoor navigation research with the Khepera III mobile robot: An experimental baseline with a case-study on ultra-wideband positioning," in *International Conference on Indoor Positioning and Indoor Navigation (IPIN)*. IEEE, 2010, pp. 1–9.

[16] P. H. Zipfel, *Modeling and Simulation of Aerospace Vehicle Dynamics Second Edition*. AIAA, 2007.

[17] R. Mahony, V. Kumar, and P. Corke, "Aerial vehicles: Modeling, estimation, and control of quadrotor," *IEEE Robotics & Automation Magazine*, vol. 19, no. 3, pp. 20–32, 2012.

[18] P. Pounds, R. Mahony, P. Hynes, and J. Roberts, "Design of a four-rotor aerial robot," in *Australasian Conference on Robotics and Automation*, vol. 27, 2002, p. 29.

[19] P. Martin and E. Salaün, "The true role of accelerometer feedback in quadrotor control," in *IEEE International Conference on Robotics and Automation (ICRA)*. IEEE, 2010, pp. 1623–1629.

[20] D. Abeywardena, S. Kodagoda, G. Dissanayake, and R. Munasinghe, "Improved state estimation in quadrotor MAVs: A novel drift-free velocity estimator," 2013.

[21] R. Leishman, J. Macdonald, R. Beard, and T. McLain, "Quadrotors and accelerometers: State estimation with an improved dynamic model," *Control Systems, IEEE*, vol. 34, no. 1, pp. 28–41, 2014.

[22] B. W. McCormick, *Aerodynamics Aeronautics and Flight Mechanics*. John Wiley & Sons, Inc, 1995.

[23] H. Huang, G. Hoffmann, S. Waslander, and C. Tomlin, "Aerodynamics and control of autonomous quadrotor helicopters in aggressive maneuvering," in *IEEE International Conference on Robotics and Automation (ICRA)*, May 2009, pp. 3277–3282.

[24] M. Bangura, H. Lim, H. Kim, and R. Mahony, "Aerodynamic power control for multirotor aerial vehicles," in *IEEE International Conference on Robotics and Automation (ICRA)*, May 2014, pp. 529–536.

[25] J. L. Crassidis, F. L. Markley, and Y. Cheng, "Survey of nonlinear attitude estimation methods," *Journal of Guidance, Control, and Dynamics*, vol. 30, no. 1, pp. 12–28, 2007.

[26] Y. Bar-Shalom, X. R. Li, and T. Kirubarajan, *Estimation with applications to tracking and navigation: theory algorithms and software*. John Wiley & Sons, 2004.

[27] J. Stuelpnagel, "On the parametrization of the three-dimensional rotation group," *SIAM review*, vol. 6, no. 4, pp. 422–430, 1964.

[28] M. D. Shuster, "Constraint in attitude estimation Part I: Constrained estimation," *Journal of the Astronautical Sciences*, vol. 51, no. 1, pp. 51–74, 2003.

[29] F. L. Markley, "Attitude error representations for Kalman filtering," *Journal of guidance, control, and dynamics*, vol. 26, no. 2, pp. 311–317, 2003.

[30] H. Soganci, S. Gezici, and H. Poor, "Accurate positioning in ultra-wideband systems," *IEEE Wireless Communications*, vol. 18, no. 2, pp. 19–27, 2011.

[31] R. Dalce, "Comparison of indoor localization systems based on wireless communications," *Wireless Engineering and Technology*, vol. 02, no. 04, pp. 240–256, 2011.

[32] H. Wymeersch, J. Lien, and M. Z. Win, "Cooperative localization in wireless networks," *Proceedings of the IEEE*, vol. 97, no. 2, pp. 427–450, 2009.

[33] D. Gurdan, J. Stumpf, M. Achtelik, K.-M. Doth, G. Hirzinger, and D. Rus, "Energy-efficient autonomous four-rotor flying robot controlled at 1 kHz," in *IEEE International Conference on Robotics and Automation (ICRA)*, April 2007, pp. 361–366.

[34] M. W. Mueller, M. Hehn, and R. D'Andrea, "A computationally efficient algorithm for state-to-state quadrocopter trajectory generation and feasibility verification," in *IEEE/RSJ International Conference on Intelligent Robots and Systems (IROS)*, 2013, pp. 3480–3486.

[35] A. Shahi, A. Aryan, J. S. West, C. T. Haas, and R. C. G. Haas, "Deterioration of UWB positioning during construction," *Automation in Construction*, vol. 24, pp. 72–80, 2012.

[36] W. Sörgel and W. Wiesbeck, "Influence of the antennas on the ultra-wideband transmission," *EURASIP J. Appl. Signal Process.*, vol. 2005, pp. 296–305, 2005.